JOURNAL OF Applied Polymer SCIENCE

Low-cost, environmentally friendly route to produce glass fiber-reinforced polymer composites with microfibrillated cellulose interphase

B. E. B. Uribe, A. J. F. Carvalho, J. R. Tarpani
Department of Materials Engineering, São Carlos School of Engineering, University of São Paulo 13566-590, Brazil
Correspondence to: J. R. Tarpani (E-mail: jrpan@sc.usp.br)

ABSTRACT: In this article, an easy, effective, and eco-friendly method to improve the mechanical performance of glass fiber-reinforced polymer composites is proposed, which involves the coating of unsized glass fiber fabric layers by simple immersion in an aqueous suspension containing sugarcane bagasse microfibrillated cellulose (MFC), followed by vacuum-assisted liquid resin infusion as the processing method. From atomic force microscopy, a 250 nm MFC-rich interphase was found, revealing its ability to build micro- and nanobridges acting as bulk epoxy matrix and GF linker. The interlaminar shear strength, quasi-static tensile, and flexural tests, as well as the morphological and fractographic inspection of test coupons containing the secondary substructure, broadly supported the assumption of the efficient role on the interfacial level of this nano reinforcement by enhancing the load transference and distribution from the polymer matrix to the main reinforcing fiber system compared to baseline unsized fiber-reinforced epoxy laminates. This finding permits this class of composite materials to be considered as having great potential to achieve products with excellent performance/cost ratios. © 2016 Wiley Periodicals, Inc. J. Appl. Polym. Sci. **2016**, *133*, 44183.

KEYWORDS: cellulose and other wood products; nanostructured polymers; self-assembly; surfaces and interfaces; synthesis and processing

Received 10 March 2016; accepted 12 July 2016
DOI: 10.1002/app.44183

INTRODUCTION

The reinforcement of polymer matrices with continuous glass fibers (GFRP) has wide applicability in fields such as the aerospace, construction, automotive, naval, wind, and oil industries, which often demand high performance materials capable of effectively supporting the loading. Recently, the improvement of composite interfaces has been one of the most important topics of great interest to researchers from different fields that involves composite science and technology, rising as a challenge the different ways of reducing processing times and costs parallel to the enhancement of the ultimate properties of composite laminates. Hierarchical structures and tailored interphases in composites have been studied in the last few years due to their positive contribution on the functional and mechanical properties, giving extensive applicability in different fields.[1–3]

A limitation of composite materials is attributed to both the interfacial adhesion between the mains phases, namely fiber and matrix, and the matrix properties surrounding the interface, aspects dominating their ultimate properties.[4]

So far, a wide variety of methods have been proposed to enhance the interfacial adhesion in GFRP composites, such as the chemical treatment of fibers and matrices. The use of functional silanes, silica, and silicates groups incrementing the affinity among phases into the composite are well known by the scientific community.[5–7] Interfacial improvements in composites can also be carried out by means of physical treatments of fibers. The use of plasma is an effective method to enhance fiber–matrix adhesion, affecting principally the chemical and physical properties of the surface layer.[8,9] Argon and oxygen gas plasmas are characterized to introduce hydroxyl functional groups, modifying the main properties of the surface,[10] although a noticeable risk of damage to the reinforcement has also been reported,[11] very probably because of long-term plasma exposure, resulting in stress concentrators introduced into the fibers' surface.

The region surrounding the fiber is the composite interphase, defined as the volumetric region that controls the interaction between the reinforcement and the matrix governing its mechanical behavior.[12,13] Its capability to bear loads depends on the physico-chemical or frictional nature of matrix/reinforcement adhesion.[13] The physico-chemical nature, related to chemical bonding and intermolecular interactions, is apparently more influential in polymer matrix composites than the frictional one, although this latter condition is often relevant.[5]

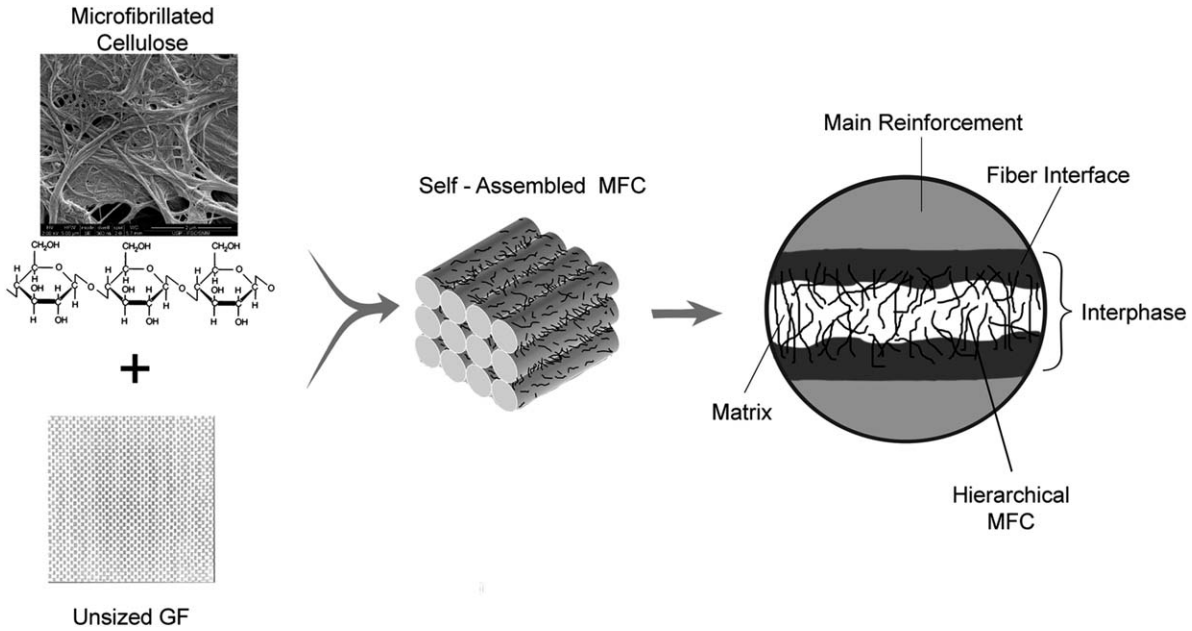

Figure 1. Schematic of the novel production route of MFC-based hierarchical GFRP laminate.

To improve the mechanical properties of the matrix near to the fiber interface, the use of nanofillers disposed in a hierarchical structure has been proposed.[4,14] The incorporation of carbon nanotubes (CNTs) as hierarchical substructures achieving higher stress resistance and toughness in the interlaminar and intralaminar regions of composites has been studied in detail.[4,15–18]

Recently, microfibrillated cellulose (MFC) has been positioned as a potential interfacial agent in fiber-reinforced plastics, with the benefits of low cost, minimal environmental impact, renewable resources, and huge availability compared to the other materials that were used in the aforementioned competing techniques.[19,20] So far, MFC has been incorporated directly into epoxy resin by solvent exchange,[21] preventing its use in cost-effective liquid resin infusion or resin transfer molding manufacturing techniques, where good flow, permeability, and wettability properties are of critical importance.[22,23]

The main purpose of this study is to reinforce the weak polymer matrix that surrounds the interfacial region, increasing the ultimate mechanical strength of GFRP. In this sense, we expect to contribute in an effective and sustainable way to the market growth of this continuous glass-fiber-reinforced polymer composite, exhibiting optimum performance/cost ratios.

EXPERIMENTAL

The MFC utilized here was synthesized from cane bagasse, described elsewhere.[24] Continuous unsized GF in the form of 0.18-mm thick bidirectional plain-weave fabric displaying areal weight of 200 g/m^2 and 1k filaments per bundle, provided by Fibertex Brazil^{TM} were employed as the main reinforcing structure in the hierarchical composite laminate. A liquid system composed of Araldite LY 1316-2 BR epoxy resin based on bisphenol A diglycidyl ether (DGEBA) monomer and Aradur HY 2963 hardener was purchased from Huntsman Brazil^{TM}. The resin was infused in both dry preforms of unsized GF (baseline material) and MFC-coated GF, respectively. Unsized (neat) GF fabric preforms were simply dipped in aqueous MFC suspension (0.1% MFC in weight) for impregnation and were subsequently dried in an oven for 3 h at 102 °C, until weight loss was negligible. Five plies with in-plane dimensions of 300 mm × 200 mm, each one comprising an unsized GF fabric covered with MFC, were piled up according to the quasi-isotropic sequence [(0/90),(±45),(0/90),(±45),(0/90)]. Two-component liquid epoxy resin system was prepared by stirring it in a mixer with an anchor-shaped propeller, followed by degassing at −93 kPa for 8 min at ambient temperature of 25 °C. Vacuum-assisted liquid resin infusion on flexible tooling was carried out using the same set of pressures and temperatures given above, giving rise in both cases to 1.0-mm thick laminates. Curing was carried out for 12 h under a vacuum bagging pressure of −50 kPa at ambient temperature. Figure 1 summarizes the basic steps of the proposed methodology to obtain MFC-based hierarchical GFRP laminates.

Test coupons were carefully and precisely machined from GFRP laminates by employing a rotating thin water-cooled diamond circular saw cutting blade. Test coupon sizes and shapes strictly followed the guidelines provided by ASTM standards: designations D3039-08 (tensile testing), D7264-08 (flexural testing), D2344 (interlaminar shear strength testing), and D7028-07 (dynamical-mechanical testing).

A microprocessor-based electromechanical universal testing machine EMIC model 23-100^{TM} equipped with a 10 kN load cell and axial extensometer with original gage length of 25 mm was utilized in monotonic tensile testing. Five full-thickness test coupons with dimensions 250 mm × 22 mm were used for each class of GFRP composite laminate, i.e., conventionally conceived and hierarchically structured. The tests were carried out under displacement-controlled conditions, with the test speed fixed at a rate of 2 mm/min.

Three-point flexural testing was conducted in the same testing machine under displacement-controlled conditions at a

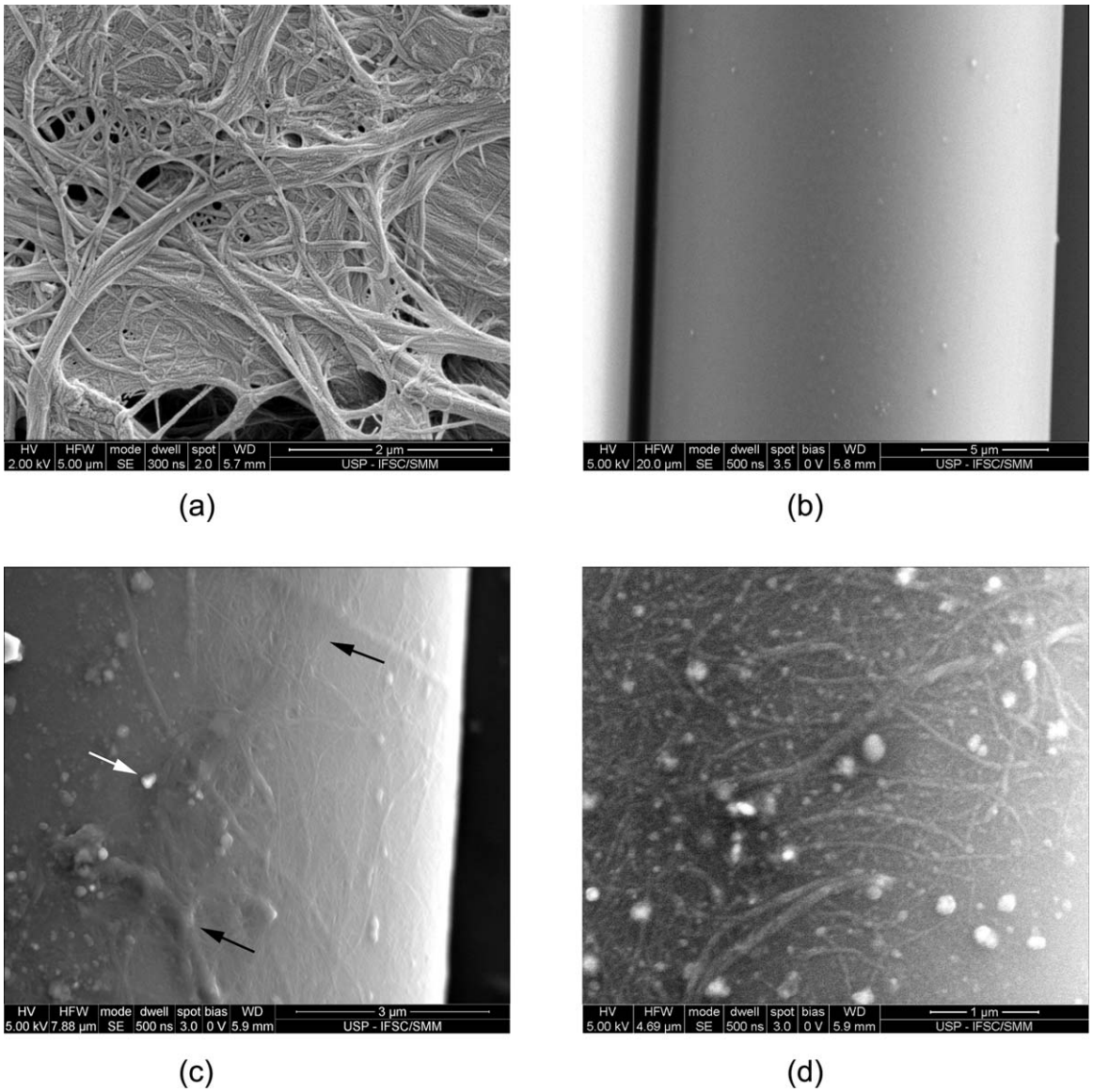

Figure 2. SEM imaging of (a) MFC morphology; (b) pristine unsized GF; (c) neat GF surface after MFC hierarchical substructure incorporation; (d) heterogeneous MFC pattern deposited over GF.

deflection rate of 1 mm/min measured at the midspan loading line. Five full-thickness test coupons with dimensions 80 mm × 10 mm were utilized for each of the two composite laminate categories. The tests were conducted employing a span length of 40 mm. A thin film of PEEK (poly-ether-ether-ketone) thermoplastic polymer was placed in between the composite test coupon and, respectively, the acting and the supporting steel-made rollers, to avoid untimely failure of the laminates by crush-inducing damage.

Interlaminar shear strength (ILSS) testing was performed using the same universal testing machine described previously by applying a central load train speed rate of 1 mm/min and employing a span length of 12 mm. Five full-thickness specimens with dimensions 18 mm × 12 mm were tested for each type of composite laminate. A thin film of PEEK polymer was placed in between the composite test coupon and, respectively, the acting and the supporting steel-made rollers, to avoid complications discussed earlier for the flexural test.

Dynamic mechanical analysis (DMA) analysis was carried out in Perkin Elmer model DMA 800^{TM} equipment operating under three-point bend mode (span length of 45 mm) with a sinusoidal waveform loading applied at a frequency of 1 Hz. A heating rate of 5 °C/min was imposed inside the chamber containing a full-thickness test piece of dimensions 50 mm × 10 mm. The temperature range of −50 to 300 °C was fully swept in order to identify clearly the respective glass transition temperatures of conventionally designed and hierarchically structured GFRP laminates. Three full-thickness specimens were tested for each of the aforementioned composites.

Height and phase imaging were simultaneously carried out in tapping mode in Brucker Atomic force microscopy (AFM)

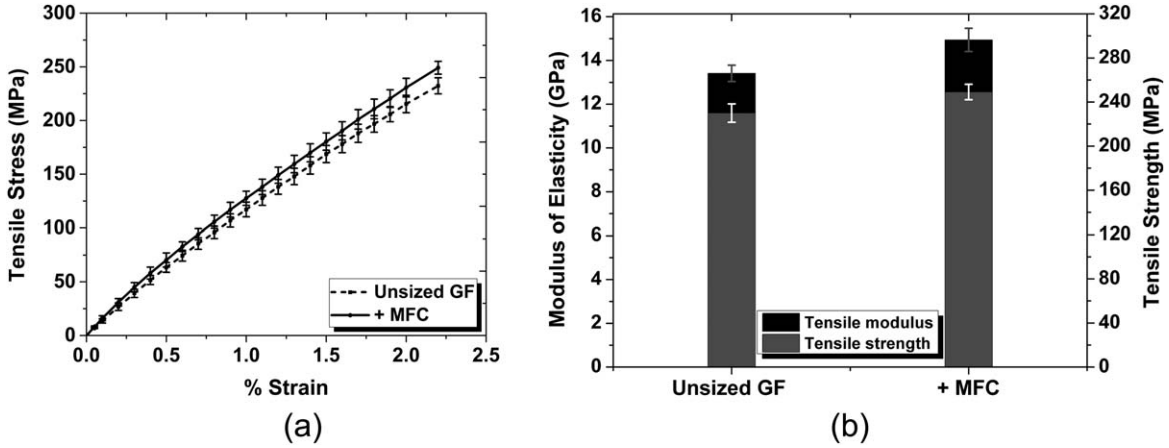

Figure 3. (a) Tensile stress–strain curves of GFRP before and after strengthening with MFC; (b) tensile modulus and strength of GFRP in both testing conditions.

MultiMode 8 SPM™ equipment with a scan rate of 1 Hz, using antimony-doped silicon probes with tip radius of 1.5 nm, drive frequency of 100 kHz, and spring constant of 5.0 N/m. In tapping mode atomic force microscopy (AFM), the cantilever is excited into resonance oscillation with a piezoelectric driver. The oscillation amplitude in the vertical direction (height imaging) is used as a feedback signal to calculate the topographic variations of the sample (i.e., surface roughness measurements), which, in turn, allows one to estimate the size of the dispersed (i.e., non-continuous) composite constituents (e.g., interphases). In phase imaging, the phase lag between the piezoelectric signal that drives the cantilever oscillation and the cantilever oscillation output signal is simultaneously monitored and recorded. The phase lag is very sensitive to variations in material properties such as composition, friction, adhesion, and viscoelasticity, which gives the possibility of characterizing quantitatively the individual components of composite materials.

In inspecting the fractographic and morphological aspects of the hierarchical (GF + MFC) epoxy resin matrix composite, a low-vacuum, high-resolution FEI Inspect F50 Field Emission Scanning electron microscopy (SEM)™ was used. The examined surfaces were previously sputter coated with electrically conductive ultra-thin layers of carbon to improve imaging quality. The secondary electron imaging mode was employed at low accelerating voltages ranging from 2 to 10 kV.

RESULTS AND DISCUSSION

MFC Deposition on the Main GF Reinforcement

Figure 2(a) shows an SEM micrograph of an MFC substructure, where its typical aspect is exceptionally large, exhibiting a web-like structure with an appreciable surface area that, in this case, depends on different factors like the fibril diameter, which has a close relationship to its porosity.[25] The appearance of this MFC frame is quite similar to the hierarchical fibrous structure found inside a turtle's carapace shell, providing it with strength, stiffness and toughness.[26]

Figure 2(b) displays continuous unsized GF in the as-received condition, while Figure 2(c) depicts the very interesting pattern obtained by compounding the MFC and GF networks, presenting a very well-adhered, thin, and homogeneously distributed MFC substructure superposing the main GF framework. The chemical interaction between the GF and MFC substructure is

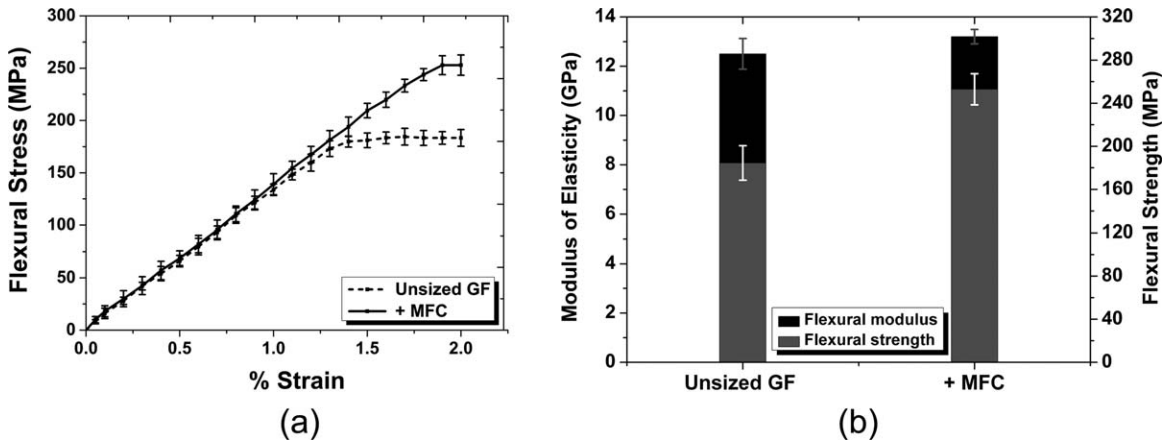

Figure 4. (a) Flexural stress–strain curves of GFRP before and after strengthening with MFC; (b) flexural modulus and strength of GFRP in both testing conditions.

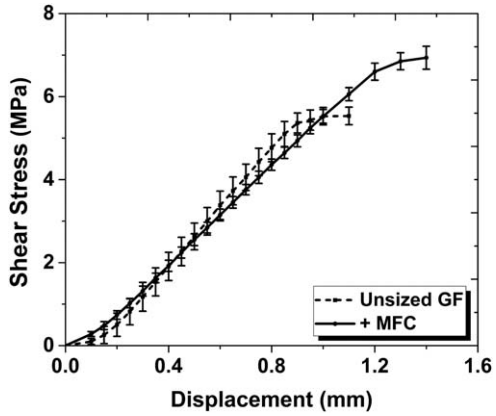

Figure 5. Interlaminar shear behavior of GFRP laminates respectively without and with the use of MFC substructure as a fiber/matrix interfacial agent.

mainly associated on the basis of hydrogen bonds between hydroxyl groups present in both the structures.

Still in Figure 2c, black arrows point out the two extremes of MFC diameters, i.e., coarse structure below and very refined above, while the white arrow indicates a contamination particle stuck to the GF. The nano-scale coalescence effect in MFC can be avoided with drying temperature control and chemical stirring during its synthesis to minimize its formation, which reduces the quality of cellulose by decreasing its strength.[27] Figure 2d allows one to appreciate the broad diameter spectrum of nanofibrils firmly attached to the GF surface; contamination particles present in unsized GF become evident as well. Several weight measurements of dry neat GF samples before and after MFC impregnation showed that the weight percentage of the latter effectively attached to the former was 0.04%, with a standard deviation of 0.01%. This remarkably low value in terms of impregnation could be associated with the facility of glass fibers to attract tiny MFC fibers over their surface, building a homogenous smooth coating as clearly depicted in Figure 2(d).

Mechanical Testing

Two averaged tensile stress–strain curves for, respectively, neat GF and neat GF + MFC reinforcing epoxy laminates are displayed in Figure 3(a). Both curves were fitted on a point-to-point basis at selected strain amplitudes, with the corresponding standard deviation of stress values given as vertical bars. The behavior in the MFC condition was similar to the baseline laminate. A slight increase in both the stiffness (+7%, with a Pearson's Coefficient of Variation—PCV of 2.2%), shown in Figure 3(b), and the ultimate tensile strength (+7%, PCV of 3.2%) indicates the relatively low efficacy of MFC incorporation in improving load transference and distribution through the matrix-fiber interface under such mode loading.

Fracture toughness in tensile tests, expressed as the area under the tensile stress–strain curve, slightly increased by 8%. This relationship was measured using the commercial data analysis software *Originlab,* Northampton, MA.

Figure 4(a) presents averaged flexural stress–strain curves for, respectively, neat GF and neat GF + MFC reinforcing epoxy resin laminates. Both curves were fitted on a point-to-point basis at selected strain amplitudes. As seen in Figure 4(b), the improvement in stiffness due to nanocellulose is close to 5%. In fact, at relatively low strain levels (below 1%), the flexural modulus in both conditions depends mainly on the matrix and the glass fibers, and only after applying higher loadings does the action of the nano- and micro-constituents of MFC restrict the interfacial mobility, controlling preferentially the ultimate properties of the laminate. As observed, the enhancement in the ultimate flexural strength shown in Figure 4(b) (+38%, PCV of 6.7%) is more than five times that of the pure tensile mode. This behavior could be related to the fact that the failure mechanisms of bent continuous GFRP depend to a large extent on compressive stresses. In this respect, the matrix is responsible for supporting the reinforcing fibers to prevent microbuckling failure in the material portion where the compressive stresses are generated.[28]

The fracture toughness was also measured in both the baseline and MFC-glass fiber coated coupon tests, this last condition resulting in an increase of 14%. These improvements can be

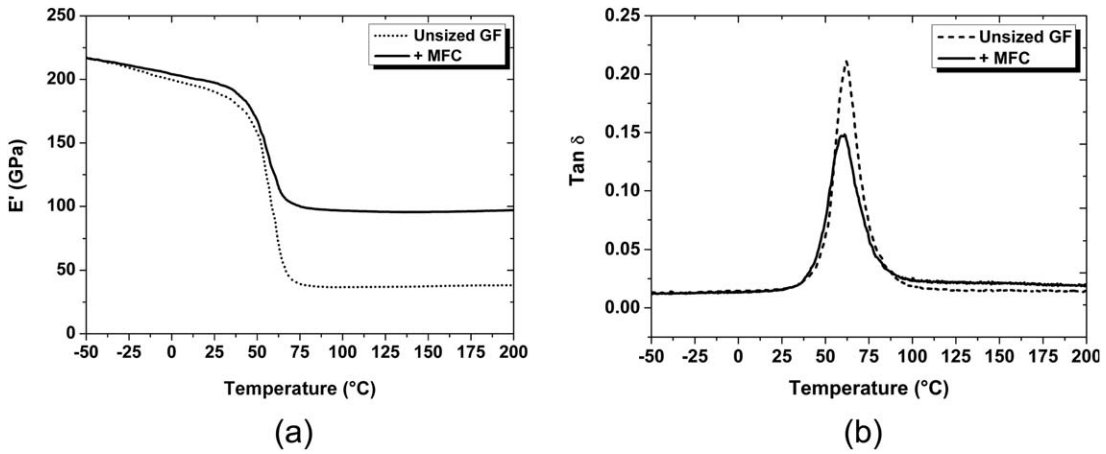

Figure 6. DMA curves displaying (a) storage modulus and (b) tan δ of GFRP laminates manufactured respectively without and with the presence of the MFC substructure as an interphase-producing agent.

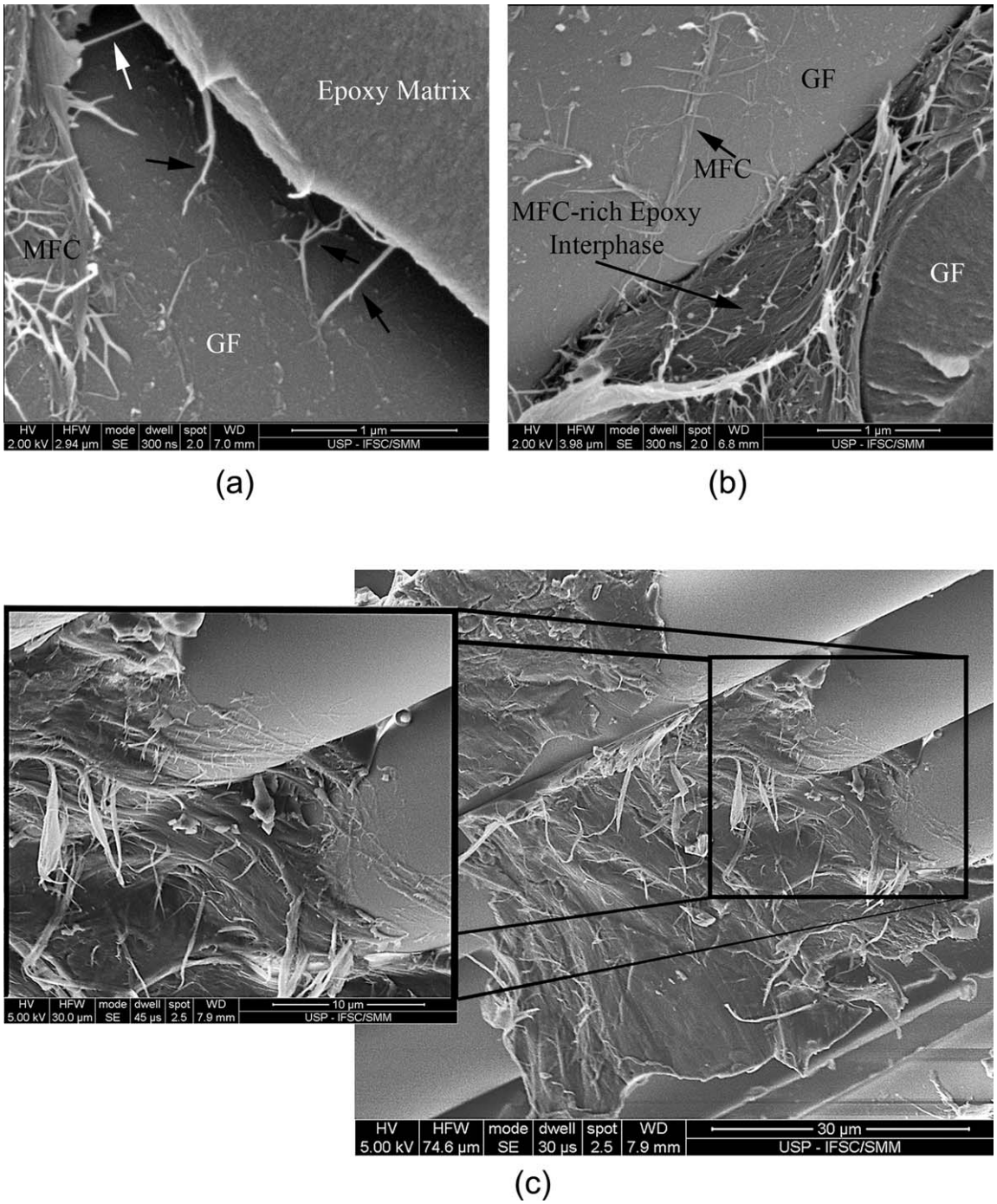

Figure 7. (a) Fracture topography of GFRP showing arrowed nanocellulose fibrils still enduring local tensile stresses acting between a portion of MFC-rich resin polymer and GF reinforcement. (b) Reliable portrait of the so-called "3D interphase"; (c) MFC-rich and MFC-free zones on the GF framework surface.

achievable only as a consequence of effective chemical and/or physical interaction of the MFC agent with both the main CF network and the enveloping thermosetting polymer matrix.

The results of ILSS for the neat GF and neat GF + MFC reinforcing epoxy resin laminates are presented in Figure 5, showing a substantial improvement of 27% in the GF + MFC condition over the baseline laminate. The fracture toughness was calculated based on the under-curve area of each condition, resulting in an increase of 60% in the MFC-coated fiber laminate. Flexural and particularly ILSS properties obtained in this study indicate that MFC incorporation may lead to the enhancement of impact properties in GFRP, since the interlaminar shear strength is one of the most important parameters determining the ability of a composite to resist delamination damage.[29]

Similar to the flexural behavior, the stiffness ratio was not improved noticeably. A slight difference of 3% in the slope of both curves was due to the minimal MFC contribution in the composite elastic region, as previously observed in the tensile and flexural moduli.

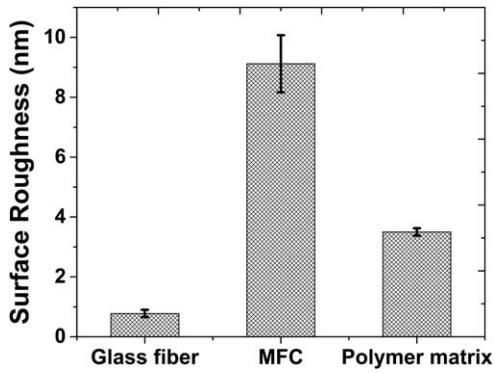

Figure 8. Average roughness (and corresponding standard deviation) of three different phases composing the hierarchical composite laminate, as resolved by AFM analysis.

The main hierarchical action inside the composite is to support the transverse load due to the thickness-oriented nanofibers,[30] resulting in a greater resistance to failure by delamination in the composite material.[31] Through hierarchical approaches, matrix-dominated properties, such as interlaminar shear strength, have been reported to improve by between 8 and 30%,[32] thus expressing the high degree of success achieved in the present work. Delamination arresting is expected to occur due to pull-out, interleaving, and bridging toughening mechanisms. According to these proposed mechanisms, MFC is likely to support shear loading by means of the thickness-oriented nanofibers, resulting in higher delamination resistance.

Dynamical Mechanical Analysis

Figure 6(a) shows the storage modulus of MFC-based laminate in the glassy state ($T \leq 25$ °C), which is much the same as that of conventional GFRP laminate. In contrast, the storage modulus in the rubbery polymer zone ($T > 75$ °C), which is strongly related to the crosslink density of neat thermosetting polymers,[33] is more than twice as high for the MFC-treated composite compared to the untreated one. In this regard, the hierarchical self-assemblage of the MFC substructure on the main GF framework surface might be decisive under fluctuating loads at higher temperatures, when the presence of the nanofiber-rich interphase will be more than compensated for the intrinsically limited stiffness of the neat GF fiber/epoxy resin laminate, due its poor interfacial adhesion above T_g.

Figure 6(b) presents the tan δ curves for baseline and MFC-treated composite laminates. The glass transition temperature (T_g) is quite similar for both conditions, reflecting the dominance of GF in determining the thermo-mechanical behavior of this class of composites. On the other hand, the incorporation of nanocellulose fibrils reduced the tan δ peak, which can probably be related to a minor extent to the slight reduction in the polymer matrix fraction compared to the untreated GF composite.[34] As previous studies[35,36] have concluded that the magnitude of tan δ is inversely proportional to interfacial adhesion in the composites, most of the observed stiffening effect is likely to be associated with the stronger fiber/matrix interfacial adhesion provided by the MFC treatment of GF, thus effectively restraining large-scale movement of polymer chains.

Fractographic Assessment

Figure 7(a) presents the tensile fracture morphology of the two-level hierarchical structure based on GF and MFC constituents. An MFC-rich resin region firmly attached to a GF is seen, as well as some nanofibers (pointed out by white and black arrows) still linking the GF and polymer matrix phases. When stress is applied to the bulk polymer matrix, load is transmitted to the MFC-rich polymer zone, therefore reducing to a large extent the energy available to fracture the weakest phase, i.e., the brittle epoxy resin. The GF MFC-coating acts directly over that vulnerable constituent surrounding the interface region.[13] In this particular domain, polymer resin failure is prone to occur in conventional composite laminates, but in the novel hierarchically reinforced structure, the nanotoughener MFC element plays a fundamental role in substantially decreasing that probability.

Figure 7(b) portrays what Kim and Mai,[37] Pegoretti *et al.*,[38] and Drzal *et al.*[39] conceived as an interphase, which means an intermediate heterogeneous volume phenomenologically very different to both the reinforcing fiber and the bulk resin. In this regard, these authors proposed that the interfacial shear strength of a fibrous polymer composite has a close relationship with the shear strength of the tridimensional fiber-surrounding resin domain, so that once this fundamental concept was definitively recognized by the scientific community, efficient hierarchical composite structures could be technologically addressed and developed to mitigate interlaminar, intralaminar, and translaminar damages, hence enhancing the whole laminate fracture toughness as well.

In fact, Figure 7(b) speaks for itself on the essential role exerted by the MFC substructure in providing effective load transference and distribution media to the main GF reinforcing framework, at the same time that nanofibrils blend into the resin matrix, therefore simultaneously strengthening and toughening the continuous phase. This guarantees a tridimensional volumetric region, where perfect integration among the three components is achieved, reflecting directly on the mechanical performance improvement of the laminate.

Figure 7(c) shows the effect of the MFC substructure within the hierarchical composite after tensile fracture, corroborating its self-assembly capability on the GF surface. Nevertheless, the MFC-free portions of GF indicate that the coating process still has to be enhanced to certificate that the entire GF surface is MFC-impregnated and liable to exhibit the highly positive effects mentioned earlier. The poor condition of MFC-GF adhesion shown in Figure 7(c) naturally leads to low interfacial toughness in GF/MFC laminates, resulting in the undermined mechanical response of the laminate as a whole, which seems particularly true under tensile loading (Section "Mechanical Testing").

Atomic Force Microscopy

Figure 8 relates the average roughness of each of the present phases in the composite laminate after treatment with MFC. It is clearly seen that the level of roughness of the fiber is low relative to the polymer matrix, because its viscoelastic nature tends to leave higher signs of plastic deformation after cutting, thus creating this wavy surface. Furthermore, the MFC exhibits high roughness relative to the other two phases due to its three-dimensional

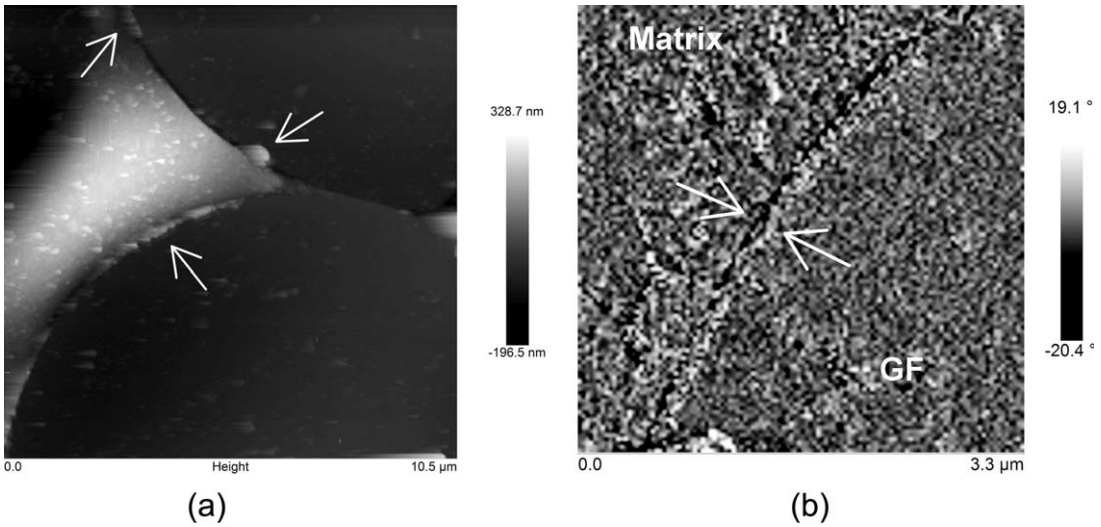

Figure 9. (a) Height and (b) phase cross-sectional 2D micrographs of the hierarchical GF + MFC reinforced epoxy matrix composite laminate.

network structure, as previously discussed in the section "MFC Deposition on the Main GF Reinforcement" [Figure 2(a)].

Figure 9(a) shows a height image of the hierarchical composite, where some MFC-rich glass edges are observed and are marked with white arrows. The region was measured at three points, resulting in an MFC thickness of 200 ± 20 nm. Due to the poor impregnation, as seen in Figure 2(c), it was not uniform over the whole fiber surface, and some fiber edges do not allow us to observe these MFC structures totally. Due to the topography created by the cutting, part of the MFC was exposed and readily observable, since it was primarily attached to the fiber. However, to find MFC linked to both the fiber and resin in order to observe the created interphase, the AFM technique was not quite satisfactory.

Phase contrast images [as shown in Figure 9(b)] are mainly associated with the adhesion characteristics, viscoelasticity, and surface area of the material and, in some cases, also reveal contrasting topographic differences in the sample.[40] This is because the phase is a measure of the dissipation of energy involved in the interaction between the tip and the material surface.[41,42] Figure 9(b) displays the MFC-rich interphase arc (marked by white arrows) created in between the matrix and the main reinforcing phase of the hierarchical composite. Figure 10 presents line scans versus the width of profile extracted from a phase and height images of the hierarchical composite performed for each measurement curve along a 1.0 micron path, starting from the epoxy polymer matrix, crossing the MFC region and ending over the GF surface. The results provide relevant information to define the three different phases clearly, in order to establish more accurately the thickness of the coated MFC layer. Both the matrix and the reinforcing phase disclosed some spikes along their measured length because of the artifacts found on the surface topography. The exhibited phase levels during the sweep of the sample denoted the interactions suffered by the cantilever during scanning of the sample, showing greater responses associated with the interfacial region.

The value of the phase width profile calculated along the region between the vertical solid lines, is much the same as that one visually estimated on the basis of Figure 9(a) and comparable corresponding to the MFC coating, was close to 200 nm. This is comparable to the height image line scan value of 250 nm measured between the pointed vertical lines, but with a slight variation possibly attributable to the type of measured property on the sample as performed via AFM microscopy. This difference of response could have been derived from some loss of information concerning the characteristics of the boundaries among both interfaces (MFC/matrix) and (MFC/reinforcement), which was not visible in the height image of Figure 9(a) nor detectable by *in-situ* phase measurements as presented in Figure 10.

CONCLUSIONS

An innovative manufacturing method to produce highly cost-effective composite laminates founded on the rapid incorporation of micro-fibrillated cellulose directly in unsized glass fiber preforms, later subjected to liquid epoxy resin vacuum-infusion, has been developed and presented.

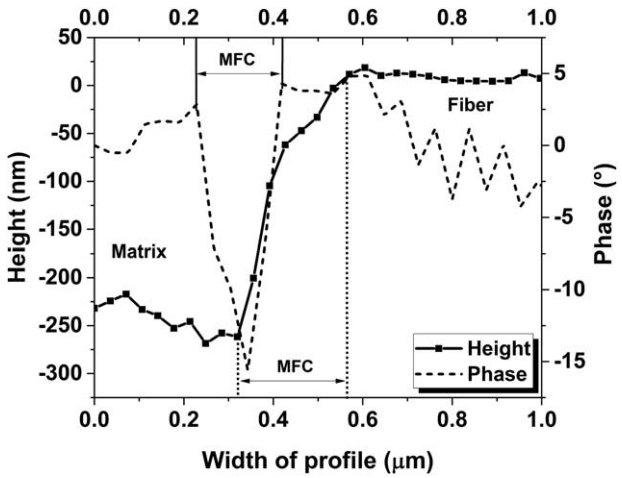

Figure 10. Phase and height line scan profiles crossing respectively the epoxy resin matrix, MFC-rich interphase and reinforcing GF of the hierarchical composite.

Having as a baseline the mechanical performance of simply unsized glass fiber laminate, stiffness gains of 38% have been attained by the hierarchically conceived composite laminate under flexural behavior. Ultimate strength increments of 38% and 27% were also attained by the novel material under flexural behavior and ILSS, respectively. The tenacity at ultimate load was increased by 60% in this latter mechanical test.

The outstanding general improvement in the mechanical performance of the glass fiber-reinforced polymer laminate is credited to the 250 nm thick micro-fibrillated cellulose-rich interphase developed in between the glass fiber and epoxy resin bulks, as thoroughly characterized and measured at nanoscale via atomic force microscope techniques. Strengthening and toughening mechanisms at the micro- and nano-levels were clearly identified and portrayed by scanning electron microscope imaging.

The results of this study are expected to contribute effectively to the market expansion of structural continuous glass fiber-reinforced polymer composites, exhibiting excellent performance/cost ratios.

ACKNOWLEDGMENTS

Authors gratefully acknowledge the scholarships provided by CNPq—Brazilian Council for Scientific and Technological Development to Uribe B.E.B. (process number 140339/2015-9), and CAPES - Coordination for the Improvement of Higher Education Personnel to Chiromito E.M.S, who helped in developing and improving the impregnation process of GF fabric with MFC.

REFERENCES

1. Yao, L.; Jiang, M.; Zhou, D.; Xu, F.; Zhao, D.; Zhang, W.; Zhou, N.; Jiang, Q.; Qiu, Y. *Compos. Part B* **2011**, *42*, 885.
2. Stickel, J. M.; Nagarajan, M. *Int. J. Appl. Glass Sci.* **2012**, *3*, 122.
3. Mäder, E.; Rausch, J.; Schmidt, N. *Compos. Part A* **2008**, *39*, 612.
4. Hui, Q.; Greenhalgh, E. S.; Shaffer, M. S. P.; Bismarck, A. *J. Mater. Chem.* **2010**, *20*, 4751.
5. Chruściel, J.; Leśniak, E. *Prog. Polym. Sci.* **2015**, *41*, 67.
6. Adeel, A.; Humaira, M. S. *Polymer* **2011**, *52*, 1345.
7. Ma, S.-Q.; Liu, W.-Q.; Hu, C.-H.; Wang, Z.-F. *Iran. Polym. J.* **2010**, *19*, 185.
8. Weikart, C. M.; Miyama, M.; Yasuda, H. K. *J. Colloid Interface Sci.* **1999**, *211*, 18.
9. John, D.; Nunnerley, C. S.; Brisley, A. C.; Sunderland, R. F.; Edwards, J. C.; Kruger, P.; Knes, R.; Paul, A. J.; Hibbert, S. *Colloids Surf. A* **2000**, *174*, 287.
10. Luner, P. E.; Oh, E. *Colloids Surf. A* **2001**, *181*, 31.
11. Ma, K.; Wang, B.; Chen, P.; Zhou, X. *Appl. Surf. Sci.* **2011**, *257*, 3824.
12. Tze, W. T. Y.; Gardner, D. J.; Tripp, C. P.; O'Neill, S. C. *J. Adhes. Sci. Technol.* **2006**, *20*, 1649.
13. Karger-Kocsis, J.; Mahmood, H.; Pegoretti, A. *Prog. Mater. Sci.* **2015**, *73*, 1.
14. Ramanathan, T.; Liu, H.; Brinson, L. C. *J. Polym. Sci. Part B: Polym. Phys.* **2005**, *43*, 2269.
15. Kim, H.; Oh, E.; Hahn, H. T.; Lee, K. H. *Compos. Part A* **2015**, *71*, 72.
16. Thostenson, E. T.; Li, W. Z.; Wang, D. Z.; Ren, Z. F.; Chou, T. W. *J. Appl. Phys.* **2002**, *91*, 6034.
17. Qian, H.; Bismarck, A.; Greenhalgh, E. S.; Kalinka, G.; Shaffer, M. S. P. *J. Am. Chem. Soc.* **2008**, *20*, 1862.
18. Godara, A.; Gorbatikh, L.; Kalinka, G.; Warrier, A.; Rochez, O.; Mezzo, L.; Luizi, F.; Van Vuure, A. W.; Lomov, S. V.; Verpoest, I. *Compos. Sci. Technol.* **2010**, *70*, 1346.
19. Chinga-Carrasco, G. *Nanoscale Res. Lett.* **2011**, *6*, 417.
20. Iwatake, A.; Nogi, M.; Yano, H. *Compos. Sci. Technol.* **2008**, *68*, 2103.
21. Gabr, M. H.; Elrahman, M. A.; Okubo, K.; Fujii, T. *Compos. Struct.* **2010**, *92*, 1999.
22. Poorzeinolabedin, M.; Parnas, L.; Dashatan, S. H. *Mater. Design* **2014**, *64*, 450.
23. Shojaei, A.; Ghaffarian, S. R.; Karimian, S. M. H. *Polym. Compos.* **2003**, *24*, 525.
24. Carvalho, A. J. F. *J. Renew. Mater.* **2014**, *2*, 118.
25. Lindström, T.; Naderi, A.; Wiberg, A. *J. Korea Tech. Assoc. Pulp Paper Ind.* **2015**, *47*, 5.
26. Chen, Q.; Pugno, N. M. *J. Mech. Behav. Biomed. Mater.* **2013**, *19*, 3.
27. Pönni, R.; Vuorinen, T.; Kontturi, E. *BioResources* **2012**, *7*, 6077.
28. Fleck, N. A. *Adv. Appl. Mech.* **1997**, *33*, 43.
29. Jaworske, D. A.; Maciag, C. NASA Technical Memorandum, 100248; Worcester, MA, **1987**, p 11.
30. Rosselli, F.; Santare, M. H. *Compos. Part A* **1997**, *28*, 587.
31. Granata, R. D.; Hartt, W.; Carlsson, L.; Mahfuz, H.; Drzal, L. 2009, http://www.dtic.mil/dtic/tr/fulltext/u2/a508406.pdf (Accessed November 5, **2015**).
32. Blaker, J. J.; Lee, K. Y.; Bismarck, A. *J. Biobased Mater. Bioenerg.* **2011**, *5*, 1.
33. Fry, C. G.; Lind, A. C. *Macromolecules* **1988**, *21*, 1292.
34. Shaffer, M. S. P.; Windle, A. H. *Adv. Mater.* **1999**, *11*, 937.
35. Mohanty, S.; Verma, S. K.; Nayak, S. K. *Compos. Sci. Technol.* **2006**, *66*, 538.
36. Ray, D.; Sarkar, B. K.; Das, S.; Rana, A. K. *Compos. Sci. Technol.* **2002**, *62*, 911.
37. Kim, J. K.; Mai, Y. W. *Compos. Sci. Technol.* **1991**, *41*, 33.
38. Pegoretti, A.; Della Volpe, C.; Detassis, M.; Migliaresi, C.; Wagner, H. D. *Compos. Part A* **1996**, *27*, 1067.
39. Drzal, L. T.; Rich, M. J.; Lloyd, P. F. *J. Adhes.* **1983**, *16*, 1.
40. Martínez, N. F.; García, R. *Nanotechnology* **2006**, *17*, 167.
41. García, R.; Tamayo, J.; San Paulo, A. *Surf. Interface Anal.* **1999**, *27*, 312.
42. Tamayo, J.; García, R. *Appl. Phys. Lett.* **1998**, *73*, 2926.